Contents lists available at ScienceDirect

Journal of Power Sources

journal homepage: www.elsevier.com/locate/jpowsour

MXene-based suspension electrode with improved energy density for electrochemical flow capacitors

Pushpendra Singh [a,b,d], Bilen Akuzum [a,d], Christopher E. Shuck [a], Kaushik Pal [b,c,*], Yury Gogotsi [a,**], E. Caglan Kumbur [d,***]

[a] A. J. Drexel Nanomaterials Institute and Department of Materials Science and Engineering Drexel University, Philadelphia, PA, 19104, USA
[b] Center of Nanotechnology, Indian Institute of Technology Roorkee, Roorkee, 247667, India
[c] Department of Mechanical and Industrial Engineering, Indian Institute of Technology Roorkee, Roorkee, 247667, India
[d] Electrochemical Energy Systems Laboratory, Department of Mechanical Engineering and Mechanics, Drexel University, Philadelphia, PA, 19104, USA

HIGHLIGHTS

- A $Ti_3C_2T_x$ suspension electrode has been prepared.
- The potential of $Ti_3C_2T_x$ for electrochemical flow capacitors (EFC) was revealed.
- A high volumetric capacitance was achieved for $Ti_3C_2T_x$ in suspension electrode.
- A novel approach for MXene-based asymmetric EFC has been explored.
- A significant improvement in the volumetric power/energy density was observed.

GRAPHICAL ABSTRACT

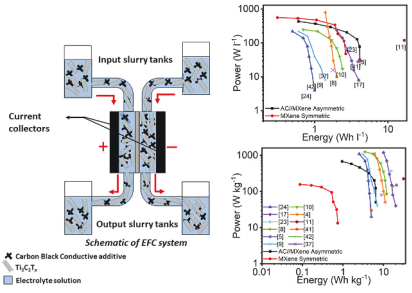

ARTICLE INFO

Keywords:
Electrochemical flow capacitors
MXene
Suspension electrodes
Energy storage
2D materials

ABSTRACT

The development of high capacitance materials with high packing density and low viscosity in suspension electrodes is critical for progressing towards high-efficiency, low-footprint electrochemical flow capacitors (EFCs). Here, we report on the first electrochemical and rheological characterization of MXene-based suspension electrodes, using multilayer $Ti_3C_2T_x$ as the active material and carbon black (CB) as the conductive additive in symmetric and asymmetric EFC devices. In the case of symmetric $Ti_3C_2T_x$ devices, the $Ti_3C_2T_x$ concentration is fixed to 22 vol.% in the slurry and the CB concentration is varied from 0.5 to 2.0 vol%. The symmetric device arrangement offers a high capacitance of 240 F ml^{-1} (2 mV s^{-1}) and volumetric energy density of 2.65 Wh l^{-1} @ power density of 47.82 W l^{-1}. Additionally, to extend the potential window, an asymmetric device assembly of activated carbon and $Ti_3C_2T_x$ is investigated. This arrangement allows a stable operating potential window of 1 V with an energy density of 4.12 Wh l^{-1} and power density of 31.73 W l^{-1}. Overall, multilayer $Ti_3C_2T_x$ seems to be excellent candidate for flowable electrode applications, offering high capacitance, energy density and low viscosity due to its high electrochemical activity, excellent electrical conductivity, and versatile surface chemistry.

* Corresponding author. Center of Nanotechnology, Indian Institute of Technology Roorkee, Roorkee, 247667, India.
** Corresponding author.
*** Corresponding author.
E-mail addresses: kaushik@me.iitr.ac.in, pl_kshk@yahoo.co.in (K. Pal), gogotsi@drexel.edu (Y. Gogotsi), eck32@drexel.edu (E.C. Kumbur).

https://doi.org/10.1016/j.jpowsour.2021.230187
Received 1 March 2021; Received in revised form 14 June 2021; Accepted 15 June 2021

1. Introduction

As renewable energy sources, such as solar or wind, become more widely used, there is an ever-increasing need for grid energy storage technologies that can cope with intrinsic power fluctuations, while being reliable and inexpensive. Electrochemical flow capacitors (EFC) [1], along with other suspension based electrochemical technologies, such as semi-solid flow batteries (SSFBs) [2] and flow-capacitive deionization (F-CDI) [3], have gained considerable attention due to their scalability and flexibility in system design. Suspension electrodes or slurry electrodes consist of a mixture of solid particles (electroactive materials and conductive additives) dispersed in electrolyte solutions [2,4,5]. Although the charge and mass transfer principles are similar for most suspension electrodes, there are major differences in the charge storage mechanism. For instance, SSFBs store energy using faradic redox mechanisms such as intercalation [2,6,7]. On the other hand, EFCs mainly store energy electrostatically via electric double layer (EDL) formation [1,8,9], as well as via fast-acting redox reaction in pseudo-capacitive materials and organic molecules [4] to improve the energy density [10,11]. Similar to redox flow batteries, EFC systems offer scalability and flexibility in system design with added advantages of high power handling capability and longer lifetime [1,5].

Coupling EFC systems with renewable energy resources can provide a cost-effective solution for intermittency issues and will accelerate their integration into urban and industrial power grids. In addition to providing robust solutions to bulk energy storage, they can also be deployed as intermediary systems to provide load-leveling and peak shaving operations against continuous power fluctuations [1,12,13]. To realize the potential of EFC systems for grid-level applications, material dependent properties such as capacitance, cycle life, energy/power output and efficiency of the operating cycle need to be improved. Moreover, the electrochemical performance of the slurry is related to the interactions between the suspended particles and the current collector, in addition to the nature of percolation networks created by the dispersed particle clusters. Correspondingly, the hydraulic efficiency of the system depends on the viscosity and flow rate of the suspension electrodes. In order to optimize the performance, a volume-spanning percolation network for low-resistance charge transfer and a high active material loading with minimal possible viscosity is necessary for low-dissipation flow [14].

To create an efficient percolation network, the solid particles should have high electronic conductivities and possess the ability to form dense aggregate structures [14]. The majority of EFC studies are based on highly conductive, high surface area carbon-based materials such as activated carbon beads, coconut-derived activated carbon, carbon nanotubes, and graphene [9,14–16]. The use of redox-active materials such as hydroquinone (HQ), p-phenylenediamine (PPD) [10,11,17] and metal oxides such as MnO_2 [4], $RuOsO_x$/graphene hybrids [18] and graphene/polyoxometalates hybrids [19] has also been reported. However, short-term degradation, limited loading of redox organic molecules, and poor electronic conductivity of metal oxides prevented further development [10,20,21]. Moreover, carbon-based materials suffer from poor dispersibility in aqueous environments due to their hydrophobic nature [22] resulting in aggregation and relatively low material loading (5–15 wt.%).

The charge percolation, coulombic efficiency, and volumetric capacitance increase with solid content in nearly all slurry electrodes, however, an excess loading of solid content makes the slurry flow dynamics impractical. Hence, there is a practical limit to how much carbon material can be loaded to suspension electrodes before the critical viscosity limit is reached [14]. The highest possible loading reported for carbon materials having a paste-like slurry consistency is around 23 wt. % [4,8,23,24]. Several attempts to increase the loading of carbon materials have been reported using various techniques. For instance, Lee et al. [26] utilized surfactants to reduce the viscosity, increasing the activated carbon loading from 16 to 23 wt.%. Hatzell et al. [25] partially oxidized the activated carbon to increase the loading from 20 to 28 wt. %, however, this oxidation caused a decrease in the electrical conductivity of the suspensions. Similarly, surfactants can also negatively impact the interconnections of the particle clusters and result in a decrease of electrical conductivity [25,26]. In this manner, exploring electrochemically active materials that easily disperse in aqueous environments and have high electrical conductivity will be promising in order to achieve high material loading in low-viscosity suspension electrodes. One class of materials that fulfills all of these requirements are MXenes.

MXenes are two-dimensional (2D) transition metal carbides, nitrides, and carbonitrides that are hydrophilic in nature and have metallic conductivity (>15,000 S cm^{-1}) [27,28]. MXenes have the general formula: $M_{n+1}X_nT_x$, where M denotes an early transition metal, X is carbon and/or nitrogen, T_x represents the surface functional groups (such as –F, –OH, –O), and n is 1–4 [29,30]. Their surface terminations result from the synthesis process, and consequently make MXenes natively hydrophilic with a redox-capable surface. In this way, MXenes enjoy the benefit of better dispersibility with low viscosity, which is harder to achieve with carbon-based materials. Furthermore, MXenes are widely used for electrochemical energy storage, with many studies demonstrating their high volumetric capacitance [28,31–33]. Moreover, rheological analysis done by Akuzum et al. [34] shows that multilayer $Ti_3C_2T_x$ MXene exhibits practical flowability even at a very high (60 wt. %) loading, making it an excellent candidate for suspension electrode applications.

In this work, we have explored the potential of multilayer $Ti_3C_2T_x$ MXene for use in flow-capacitor applications to achieve high volumetric capacitance with improved rheological properties in capacitive suspension electrodes. Concentrations up to 60 wt.% were investigated in a symmetric device configuration, corresponding to ~22 vol.% $Ti_3C_2T_x$. The volume fraction of the conductive carbon black (CB) additive was systematically varied from 0.5 to 2.0 vol% in increments of 0.5 vol.% to understand its effect on the MXene performance. Carbon black can assist in creating a percolation network, because large size of MXene particles and repulsion between negatively charged MXene particles lead to a low conductivity of MXene slurry, in spite of high metallic conductivity of individual MXene sheets. Moreover, a systematic rheological analysis has been completed to determine the viscosity of $Ti_3C_2T_x$/CB suspensions and optimize the flow performance. Furthermore, to increase the operating voltage window from 0.4 V to 1 V, we prepared activated carbon (AC) and $Ti_3C_2T_x$-based asymmetric EFC devices. The electrochemical performance of different composite slurries was evaluated using common electrochemical characterization techniques, including cyclic voltammetry, galvanostatic cycling, impedance spectroscopy, and DC conductivity analysis.

2. Materials and methods

2.1. Materials

YP-80F activated carbon (particle size 1–10 μm, Kuraray Chemicals Co.), sulfuric acid (H_2SO_4; 98 wt.%, Alfa Aesar) and acetylene carbon black (particle size ~ 0.042 μm, >99.9%, Alfa Aesar), hydrochloric acid (HCl; 37 wt.%, Sigma Aldrich), Ti_3AlC_2 MAX phase (<100 μm, Carbon-Ukraine), and hydrofluoric acid (HF; 48–51 wt.%, Acros Organics) were used. Celgard-3501 (64 nm pore size, Celgard) was used as a separator. For all experiments, deionized (DI) water (15 MΩ resistivity) was used.

2.2. Synthesis of multilayer MXene

To produce 30 g multilayer $Ti_3C_2T_x$, the scalable MXene synthesis methodology was utilized [35]; briefly 30 g Ti_3AlC_2 was added to 600 mL of 30 wt.% HF solution in a 1 L MXene etching reactor (Carbon, Ukraine) over the course of 10 min. The mixture was stirred at 150 rpm for 3 h, with water continuously following through the reactor cooling

jacket to maintain a temperature of 35 °C. Once the reaction was complete, the $Ti_3C_2T_x$ powder was transferred to four 1 L centrifugation tubes. This mixture was repeatedly washed with DI water and centrifuged at 3500 rpm for 5-min cycles until the mixture reached neutral (>6) pH. Following this, excess water was removed via vacuum filtration, then immediately used for further experiments [36].

2.3. Cell design and assembly

All electrochemical performance analysis was done under static conditions to assess the electrochemical performance of $Ti_3C_2T_x$ suspensions. For electrochemical testing, a custom made cell consisting of glassy carbon current collectors was used as shown in Fig. 1. A latex gasket was used to make a circular channel of 4 mm radius and 0.75 mm thickness to hold the slurry. The effective channel depth was 0.62 mm after arranging the cell. The celgard separator was used to separate the cathode and anode portion of the static cell. For the symmetric cell assembly, both channels were loaded with the same slurry, whereas for the asymmetric device, the $Ti_3C_2T_x$ based slurry was used as the anode and activated carbon-based slurry as the cathode.

2.4. Slurry preparation

Both, the active material and conductive additives, were added to degassed DI water and mixed with a IKA T18 digital Ultra Turbomax shear mixer at 20,000 rpm for 5 min to uniformly disperse and break up particle agglomerations. Afterwards, H_2SO_4 was added to the mixed suspensions to achieve 1 M concentration for the electrolyte. Then, this dispersion was stirred at room temperature overnight at 400 rpm to create a homogeneous slurry. This protocol was followed for all slurry compositions investigated in this study. For the symmetric device, the $Ti_3C_2T_x$ concentration was fixed to 22 vol.%. Different volume fractions (from 0.5 to 2.0 vol.% with increments of 0.5 vol.%) of carbon black were investigated as a conductive additive.

For the asymmetric configuration, 23 wt.% total carbon loading with 9:1 wt ratio of activated carbon (YP–80F) to carbon black slurry was used at cathode. This concentration was used as the reference composition because previous literature demonstrated that this concentration has the highest possible loading for achieving good capacitive performance [4]. On the other hand, an optimized 9.2 vol.% MXene and 3.4 vol.% carbon black was used as the anode slurry in asymmetric configuration. The optimization of MXene concentration was done against the carbon slurry (9:1 wt ratio of AC:CB with total weight fraction of 23 wt.%) arranged at the cathode part in two electrode cell and at counter electrode in 3-electrode cell (Fig. S4 and Fig. 6 (a)) of the cell. *Density = Weight/Volume* of MXene was taken as 3.6 g cm^{-3} (as calculated in supporting information Fig. S1), activated carbon – 0.495 g cm^{-3} and carbon black – 2.1 g cm^{-3}, respectively.

3. Characterization

SEM analysis was done using a field emission electron microscope (Zeiss VP5 Supra). To reduce sample charging, platinum/palladium was sputtered onto the surface 40 s at 40 mA (Cressington Scientific 108 Auto). X-ray diffraction (XRD) patterns were acquired for Ti_3AlC_2 and 30 wt.% HF etched multilayer $Ti_3C_2T_x$ using a powder diffractometer (Rigaku Smart Lab, Japan) with Cu Kα radiation from 5 to 90° 2θ using a step scan of 0.4° and scan speed of 1°/min. Viscosity measurements for all the prepared slurry compositions were tested using a hybrid DHR-3 Discovery rheometer (TA Instruments) gap height was kept constant at 1 mm and 20 mm cross-hatch parallel plate geometry attachments were used to avoid any wall slip.

3.1. Electrochemical measurements

Electrochemical analysis was done with a BioLogic VMP3 electrochemical workstation at room temperature. To evaluate the electrochemical performance, cyclic voltammetry (CV), galvanostatic charge discharge (GCD), electrochemical impedance spectroscopy (EIS), and DC conductivity analysis were performed. For the symmetric device configuration, electrochemical analysis was conducted for an optimized potential window of 0.4 V (see supporting information Figure S2) with CV scan rates of 2, 5, 10, 20, 50, 100, 200 mV s^{-1} and electrochemical impedance spectroscopy (EIS) for a frequency range of 1 MHz–5 mHz, respectively. In addition to that, galvanostatic charge discharge (GCD) analysis has been also performed. The slurry volume in the symmetric configuration of the cell was constant for both compartments. Volumetric/gravimetric electrode capacitance for the symmetric system was calculated using the formula:

$$C_{sp} = \frac{2\int idV}{\Delta V \times \nu \times (active\ material\ volume\ or\ mass\ in\ one\ electrode)} \quad (2)$$

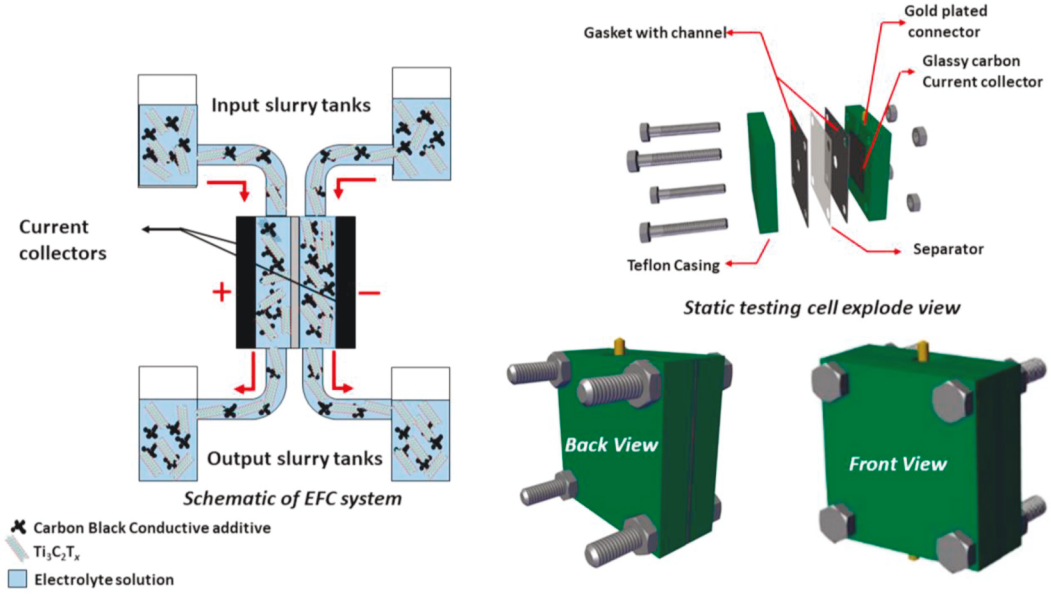

Fig. 1. Schematic of the EFC system (left), static flow cell assembly in exploded (right top) and assembled mode (bottom right).

where ΔV is the voltage wndow and ν is the scan rate.

To prepare an asymmetric device, mass balancing approach proposed by Tian et al. [37], has been adapted. In this method, the electrochemical performance of 23 wt.% carbon slurry electrodes was first investigated using a three-electrode electrochemical setup, where a silver chloride coated silver wire (preparation protocol in figure S3) was arranged between two separator membranes, acting as the pseudo-reference electrode (supporting information figure S4). After determining the capacitive performance of the carbon electrodes, the same three-electrode cell was used to characterize the individual electrode contributions to electrochemical performance. To equilibrate the electrochemical performance between $Ti_3C_2T_x$ and the carbon-based slurry electrodes, we limited the $Ti_3C_2T_x$ concentration to 9.2 vol.% and increased the CB concentration to 3.4 vol.% (supporting information figure S5). This specific balancing was done to increase the electrical conductivity by filling the gap between $Ti_3C_2T_x$ particles to maintain a percolation network for effective charge transfer. Despite the low amount of $Ti_3C_2T_x$ in the asymmetric device, this composition provides similar charge stoarge to the 23 wt.% all carbon slurry at positive electrode while allowing the electrical conductivity to reach 20 mS cm^{-1}.

For the asymmetric device configuration, similar to symmetric device electrochemical performance analysis was done at CV scan rates of 2, 5, 10, 20, 50, 100, 200 mV s^{-1} for an optimized potential window of 1 V. Moreover, EIS analysis for asymmetric device was done for a frequency range from 1 MHz to 5 mHz, respectively.

Volumetric/gravimetric capacitance of two-electrode asymmetric device was calculated using the formula:

$$C_{sp} = \frac{\int idV}{\Delta V \times v \times (\textit{active material volume or mass in both electrodes})} \quad (3)$$

where ΔV is the potential window and v is the scan rate.

For energy and power density calculation of symmetric/asymmetric device, the flowing formulae were used:

$$P = \frac{E}{t} \quad (4)$$

$$E = \frac{1}{2} C_{sp} (\Delta V)^2 \quad (5)$$

where t denotes the time taken for the discharge, C_{sp} is the device specific capacitance, ΔV is the potential window under consideration.

4. Results and discussion

4.1. Materials characterization

Fig. 2 (a,b) shows characteristic SEM images of the multilayer $Ti_3C_2T_x$. From these, the accordion-like open structure that results from etching in high wt.% HF is evident. This open structure provides accessibility to the electrolyte deep inside the layered structure, minimizing the charge transport resistance of flowable electrode slurries. Fig. 2(c) shows the XRD patterns of Ti_3AlC_2 and $Ti_3C_2T_x$. From this, the (002) peak for Ti_3AlC_2 (9.84°; d-space of 8.98 Å) shifts to the left (8.68°; d-space of 10.18 Å), indicating successful etching. This implies that some $Ti_3C_2T_x$ sheets have intercalated water, while others are dry. Furthermore, the (002) peak of Ti_3AlC_2 is absent after etching, indicating complete conversion of all MAX [32].

4.2. Rheological analysis

To better understand the suitability of $Ti_3C_2T_x$ for flowable electrode applications, it is important to understand the rheological characteristics of $Ti_3C_2T_x$ slurries. Using a cross-hatch 20 mm parallel plate geometry, the viscosity was measured from 0.001 to 100 s^{-1} shear rate.

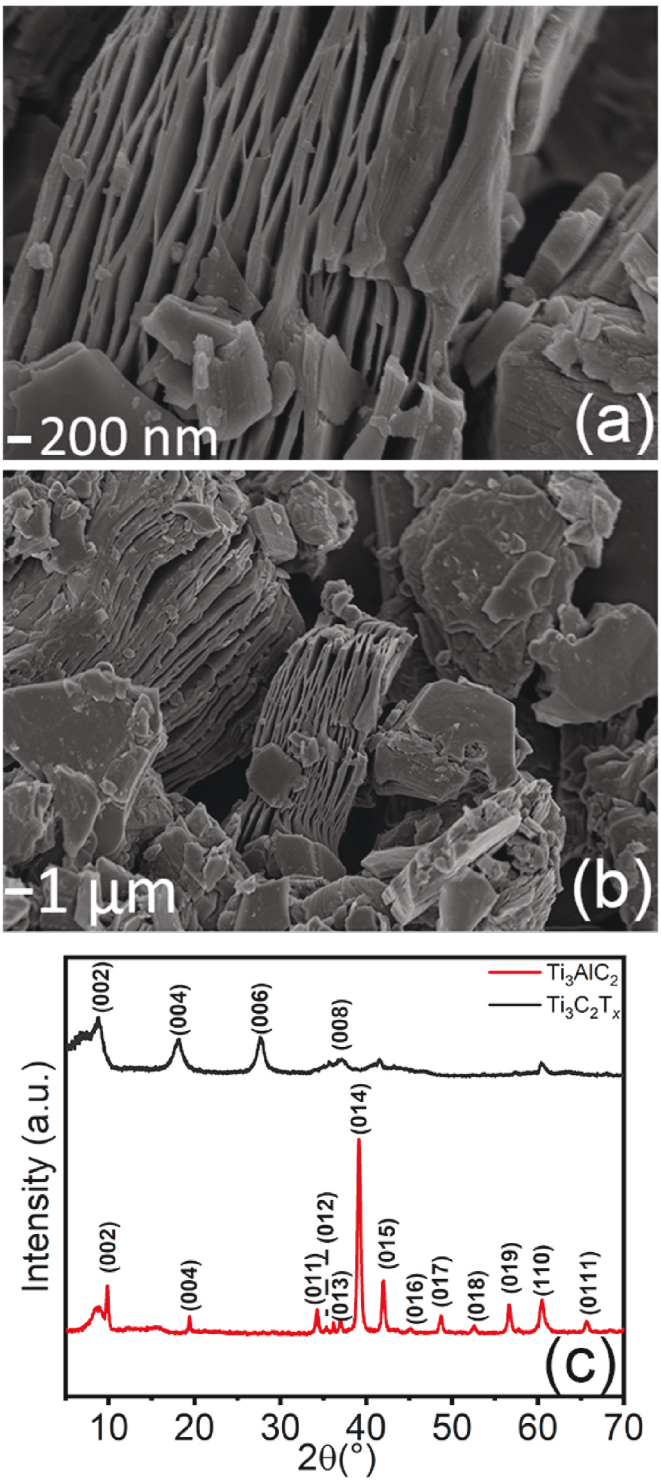

Fig. 2. SEM images of $Ti_3C_2T_x$ (a), (b) and XRD patterns of Ti_3AlC_2 and $Ti_3C_2T_x$ (c).

The morphology of the particles under investigation is shown in Fig. 2(a, b) & Figure S6 (a,b), respectively. For rheological measurements, the $Ti_3C_2T_x$ loading was kept constant at 22 vol.% with CB compositions varied. From Fig. 3, all studied slurries exhibit shear-thinning behavior, similar to previous reports on multilayer MXene rheology [34]. At the lowest CB concentration (0.5 vol.%), the low shear viscosity (0.001 s^{-1}) is 342 Pa s. As more CB is added to the slurry, the low shear viscosity drastically increases to a maximum of 113,457 Pa s at 2.0 vol.% CB. This increase in viscosity can be attributed to the facile agglomeration

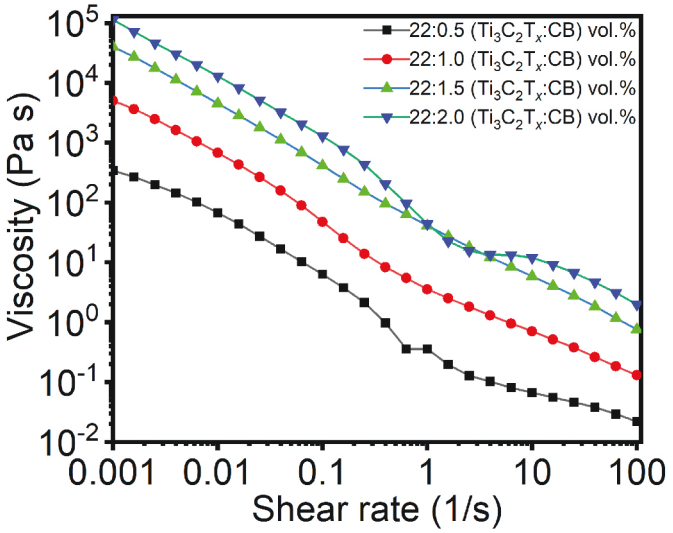

Fig. 3. Rheology data showing the variation in viscosity vs. shear rate for various volumetric percentages of CB in 22 vol.% $Ti_3C_2T_x$ slurry.

kinetics of CB particles, which begins to inhibit flow even at very dilute concentrations [14]. Correspondingly, at high loadings of 22:2.0 vol.% $Ti_3C_2T_x$:CB (56 wt.%, total solid content), the rheological behavior of the slurry is similar to 17 wt.% [38] to 23 wt.% [23] carbon slurries. Even with the addition of conductive carbon additives, the $Ti_3C_2T_x$ slurry electrodes allow higher material packing and lower resistance to flow.

4.3. Electrochemical and capacitive characterization

To understand the electrochemical performance, symmetric and asymmetric device configurations were investigated. For the symmetric configuration, slurries with the same composition were loaded into both compartments of the device (Fig. 1). Different MXenes may have different potential windows [39] but in our case, due to the limited stability of $Ti_3C_2T_x$ under positive potentials, the stable potential window for the symmetric device was set to 0.4 V. Hence, to increase the potential window, a mass balance approach was established with slight changes in the method reported by Tian et al. [37], and an asymmetric device assembly of AC//MXene suspension was investigated. The electrochemical performance of the system was normalized using the vol./wt. of the active material in the slurry electrodes unless otherwise specified. A comparative analysis was also included (Fig. 4(c)), which shows the changes in the electrochemical performance when volumetric normalization is carried out by including inactive components of the slurry.

4.3.1. Symmetric configuration

For the symmetric device, the electrochemical performance of 22 vol.% $Ti_3C_2T_x$ slurries with CB loadings from 0.5 to 2.0 vol.% were investigated. Fig. 4(a) shows the CV curves with different CB loadings and 22 vol.% $Ti_3C_2T_x$. The calculated capacitances for the symmetric devices are 34.4, 93.7, 165.8, and 240 F ml^{-1} for 0.5, 1.0, 1.5, and 2.0 vol.% CB, respectively. From Fig. 4(a), the CV curves become more rectangular as the carbon black content increases, suggesting decreased electrode resistance. Moreover, Fig. 4(b) shows that the CB additives improve the symmetric device rate performance. Fig. 4(c) illustrates the capacitance variation with CB concentration for different volumetric calculations. In this system, the capacitance can reach 240 F-ml^{-1} when normalized by the volume of the active material (i.e., $Ti_3C_2T_x$). This means that, when sufficient electrical percolation is present, aqueous suspensions of multilayer $Ti_3C_2T_x$ exhibit high electrochemical activity, proving to be a promising candidate for flow applications.

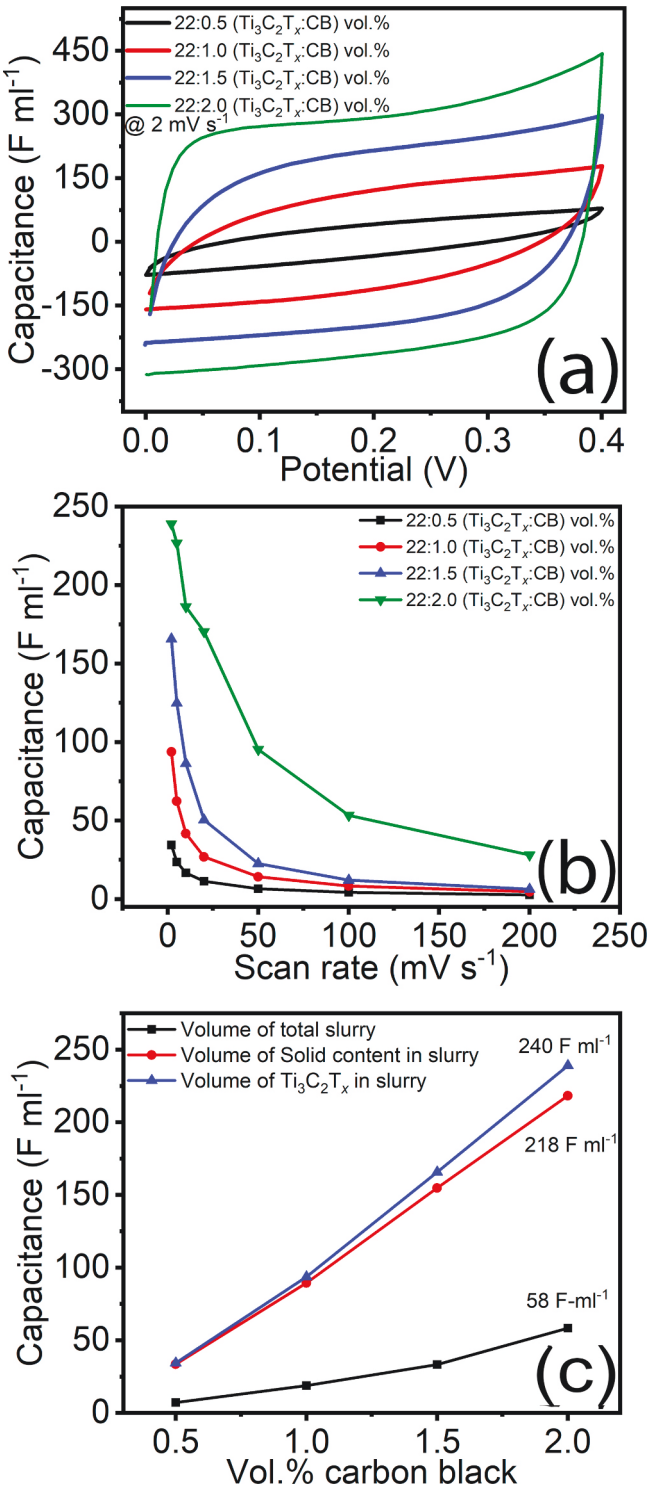

Fig. 4. Cyclic voltammetry at 2 mV s^{-1} and capacitance vs. scan rate (a), (b); Capacitance variation (at 2 mV s^{-1}) with respect to vol.% carbon black normalized to different slurry components (c).

The gravimetric capacitance was calculated for all compositions, as shown in Fig. 5(a). Due to the higher density of $Ti_3C_2T_x$ (3.6 g cm^{-3}) relative to CB (2.1 g cm^{-3}), the gravimetric performance is lower when normalized by the weight. However, for large-scale grid energy storage, the weight of the active material is not a crucial factor due to the stationary system design. Nonetheless, the highest gravimetric capacitance (66 F g^{-1}) was observed for 2.0 vol.% CB loading. Fig. 5(b) shows constant current response of all slurry compositions at ~0.22 A ml^{-1}. An

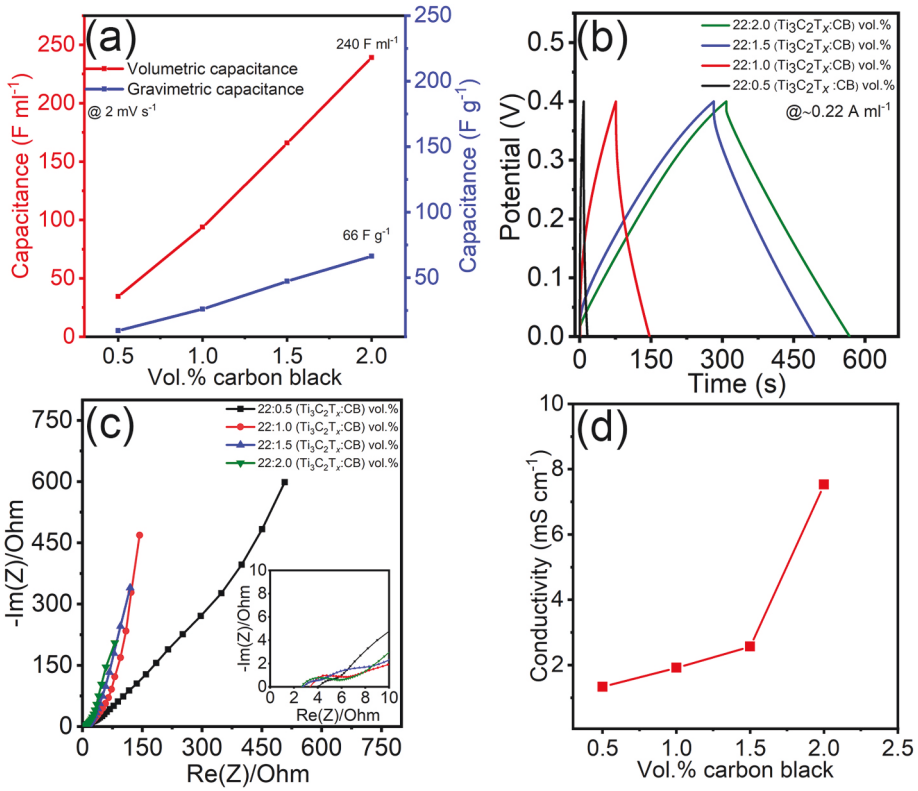

Fig. 5. Gravimetric and volumetric capacitances of symmetric device (a); GCD at ~0.22 A ml^{-1} (b); Nyquist plots for all slurry compositions from 1 MHz to 5 mHz (c). DC conductivity analysis of MXene slurries (d).

increase in the charge-discharge time with an increase in volume loading of CB is apparent in Fig. 5(b). Moreover, a reduction in the IR drop is also apparent, suggesting an increase in the slurry conductivity. While the gravimetric capacitance of $Ti_3C_2T_x$ slurries appears to be similar to activated carbon, the volumetric performance of $Ti_3C_2T_x$ is significantly better (Table 1).

Table 1 lists materials commonly used for electrochemical flow capacitors along with their electrochemical performance metrics. Because there are several different ways to normalize electrochemical data for slurry electrodes, only studies with similar normalization protocols are listed. Table 1 shows that the gravimetric performance of $Ti_3C_2T_x$ slurry electrodes is moderate compared to other capacitive materials, such as activated carbon beads. However, when the performance is normalized to the active material volume, the $Ti_3C_2T_x$ slurry volumetric capacitance outperforms all other materials [4,8]. Fig. 5 (c, d) shows the variation of slurry resistance with the addition of CB. As CB is added, the slurry conductivity increases, however, it is important to note that the absolute electrical conductivity values are lower than typical carbon-based suspensions (~50–100 mS cm^{-1}). Moreover, electrochemical impedance spectroscopy (EIS) data suggest that diffusion resistance also decreases with increasing CB. Decrease in the diffusion resistance, and corresponding increase of DC conductivity (Fig. 5(d)), can be associated with an enhanced percolation network due to the increased number of particles in the slurry. The intercept with the x-axis in the Nyquist plot in Fig. 5(c) exhibits the equivalent series resistance (ESR) for various slurry compositions: 4.07 Ω (22:0.5 vol.%), 3.2 Ω (22:1.0 vol.%), 2.7 Ω (22:1.5 vol.%), and 2.4 Ω (22:2.0 vol.%) slurry. Moreover, with increased CB content, the semicircle of EIS curves becomes more depressed and shifted to a lower resistance region, which might be a result of lower ion transportation distance between particles [40].

4.3.2. *Activated carbon (AC)//MXene asymmetric device configuration*

The capacitive performance of $Ti_3C_2T_x$ suspension electrodes surpasses conventional activated carbon slurries, as shown in Table 1. However, the operating voltage window of the symmetric $Ti_3C_2T_x$ flow capacitor is limited to 0.4 V due to the instability of $Ti_3C_2T_x$ at higher positive potentials (supporting information Fig. S2). Hence, an asymmetric device using suspensions of activated carbon for the positive electrode was investigated as an alternative approach to improve the operating voltage window and energy density. For the asymmetric device assembly, mass balancing is key to prevent loss of capacitance while extending the electrochemical device potential window. The asymmetric device in this study was prepared using activated carbon slurry as the cathode and $Ti_3C_2T_x$ slurry as the anode. A previously reported composition of activated carbon slurry electrode was utilized [4], which showed that 23 wt.% carbon slurry electrode with 9:1 wt ratio of AC:CB is optimal for flow capacitor applications. This concentration reaches the upper limit of flowability for carbon suspensions and exhibits a paste-like consistency when prepared with YP-80F activated carbon.

It was shown (figure S5) that for 9.2 vol.% MXene and 3.4 vol.% CB ratio, the capacitance offered by the MXene suspension (negative) electrode closely matches with the AC (positive) electrode capacitance. Fig. 6(a, b) and Fig. 6(c) show the voltage window and corresponding Coulombic efficiencies. Fig. 6(c) shows that, as the potential window is expanded, the Coulombic efficiency decreases; the minimum observed was 87% at a voltage of 1.2 V. At 1 V, the Coulombic efficiency was ~92%; this was chosen as the voltage window for further analysis of the AC//$Ti_3C_2T_x$ asymmetric flow capacitor.

Fig. 7(a) shows the asymmetric device CVs at various scan rates. The highest volumetric capacitance observed for the asymmetric device was 29.07 F ml^{-1} (46.58 F g^{-1}) or 29.07 C ml^{-1} (46.58 C g^{-1}). The asymmetric device capacitance is lower than that of the symmetric $Ti_3C_2T_x$ flow capacitors. This is due to the reduced $Ti_3C_2T_x$ concentration (9.2 vol.%) in the asymmetric device, which limits the capacitive performance. However, this shows that a small amount of $Ti_3C_2T_x$ (9.2 vol.%) is capable of matching the charge capacitance of high-concentration (35

Table 1
Comparison with previously reported EFC devices.

Material	Electrolyte	Capacitive performance	Reference
Carbon beads	1 M Na_2SO_4	125 F g^{-1} (24 F ml^{-1}) with CA[a] (0.6 V)	[1]
Carbon beads	1 M Na_2SO_4	92 ± 10 F g^{-1} (18 ± 2 F ml^{-1}) @5 mV s^{-1}	[23]
Carbon beads + PPD[b]	2 M KOH	~120 F ml^{-1} @ 2 mV s^{-1} ~225 F g^{-1} @ 2 mV s^{-1}	[11]
CO_2 Activated carbon beads	2 M KOH	139 F g^{-1} (27.8 F ml^{-1}) @ 2 mV s^{-1}	[24]
MnO_2 (Density) Symmetric and MnO_2//YP-50F asymmetric carbon device	1 M Na_2SO_4	149 F g^{-1} (55.13 F ml^{-1}) for symmetric device of MnO_2 @ 2 mV s^{-1}	[4]
Carbon beads	1 M H_2SO_4	154 F g^{-1} (30.8 F ml^{-1}) @ 2 mV s^{-1}	[8]
YP-50F	1 M Na_2SO_4	100 F g^{-1} (35 F ml^{-1}) @ 2 mV s^{-1}	[41]
YP-50F activated carbon	1 M Na_2SO_4	30 F ml^{-1} with CA[a] (1 V)	[5]
1. Carbon beads	1. 1 M H_2SO_4+ 0.2 M (HQ)[b]	1. 322 F g^{-1} (64.4 F ml^{-1}) @ 2 mV s^{-1}	[10]
2. Carbon beads + HQ[c]	2. 1 M H_2SO_4	2. 342 F g^{-1} (68.4 F ml^{-1}) @ 2 mV s^{-1}	
YP-80F + MWCNT	1 M Na_2SO_4	80.2 F g^{-1} (16.04 F ml^{-1}) @ 2 mV s^{-1}	[42]
rGO@Carbon beads	1 M H_2SO_4	200 F g^{-1} (~40 F ml^{-1}) @ 2 mV s^{-1}	[9]
YP-50F + 5 mm (SLS)[d]	1 M Na_2SO_4	26 F ml^{-1} with CA[a] (0.6 V)	[26]
Carbon beads	2 M KCl	100 F g^{-1} (20 F ml^{-1}) @ 2 mV s^{-1}	[37]
YP-80F	1 M Na_2SO_4	83 F g^{-1} (41.08 F ml^{-1}) with CA[a] (1 V)	[38]
MXene symmetric electrode and AC// MXene asymmetric device	1 M H_2SO_4	**$Ti_3C_2T_x$ symmetric electrode**, 240 F ml^{-1} or 66 F g^{-1} @ 2 mV s^{-1} **AC//$Ti_3C_2T_x$ asymmetric device**, 29.07 F ml^{-1} (46.58 F g^{-1}) or 29.07 C ml^{-1} (46.58 C g^{-1}) @ 2 mV s^{-1}	This work

Tap density of materials: Carbon beads (0.2 g cm^{-3}), YP-50F (0.35 g cm^{-3}), YP-80F (0.495 g cm^{-3}), MnO_2 (0.37 g cm^{-3}).
[a] Chronoamperometry.
[b] p-phenylenediamine.
[c] Hydroquinone.
[d] Sodium lignosulfonate.

vol.%) activated carbon slurry. Hence, substitution of a higher capacity active material on the positive electrode should allow the $Ti_3C_2T_x$ asymmetric device to increase its capacitance while maintaining a wider operating voltage window.

From Fig. 7(b), the rate capability of the asymmetric device is slightly better, retaining more than 90% capacitance at 10 mV s^{-1} with respect to 2 mV s^{-1}, which is only 70% in case of the symmetric device. The improvement in rate capability can be attributed to the improved electrical conductivity of the slurry as CB is added, and is also evident from the EIS curve shown in Fig. 7(c). The intercept from the x-axis in the high-frequency region shows ESR value of 1.23 Ω. However, the asymmetric device diffusion resistance is higher than the 22:2.0 vol.% symmetric configuration, which can be attributed to the porous structure of activated carbon particles, contributing to the ion transport resistance.

4.3.3. Power and energy density analysis

Fig. 8(a and b) presents the Ragone plots of the symmetric and asymmetric $Ti_3C_2T_x$ flow capacitors along with previously reported studies on flow capacitors. Since the majority of flow capacitor studies

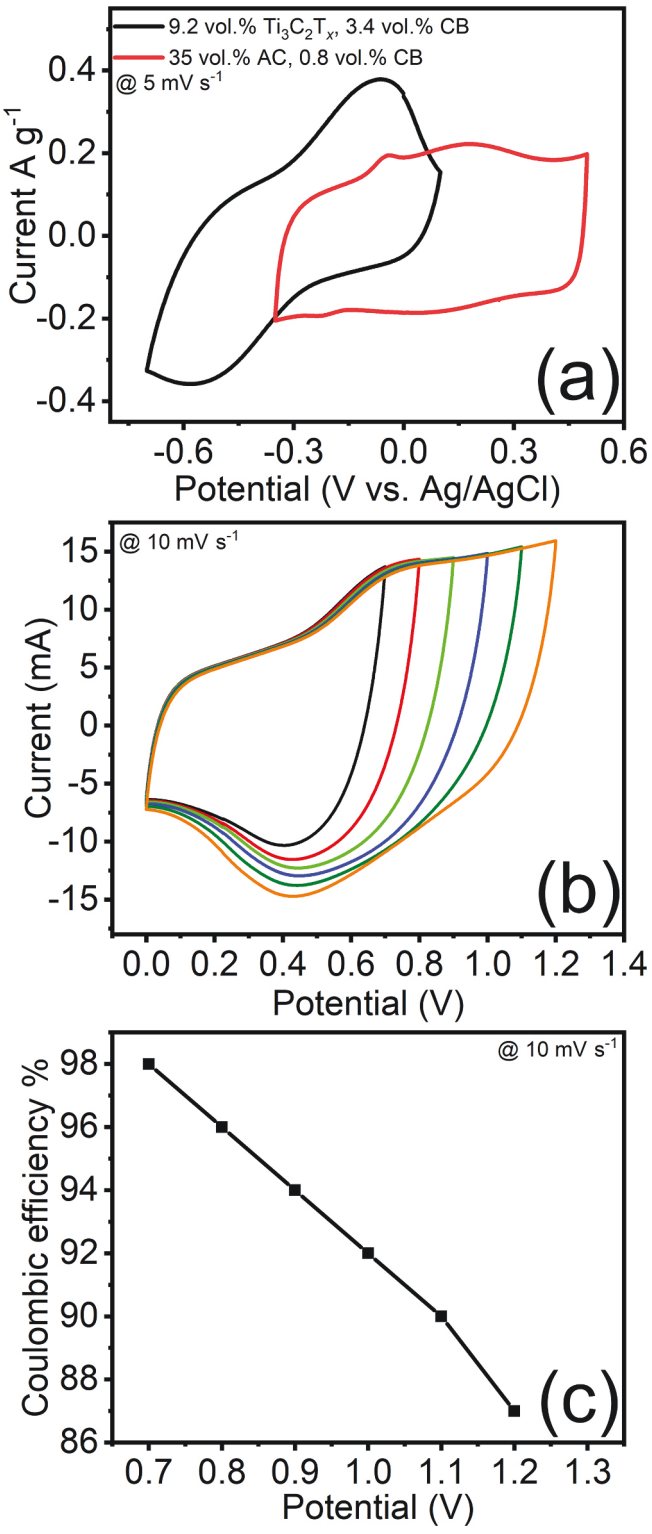

Fig. 6. Potential window test for (9.2:3.4 vol.%) $Ti_3C_2T_x$:CB and 23 wt% (9:1 ratio or 35:0.8 vol.%) Activated carbon:CB (a); voltage window test for the AC//$Ti_3C_2T_x$ asymmetric device (b); variation of Coulombic efficiency with the voltage window (c).

publish performance metrics in gravimetric units, the gravimetric energy/power density values were converted into volumetric units using the active material density reported in their respective studies. From Fig. 8(a), the volumetric power density of the symmetric $Ti_3C_2T_x$ flow capacitors outperforms existing devices, while offering a high energy

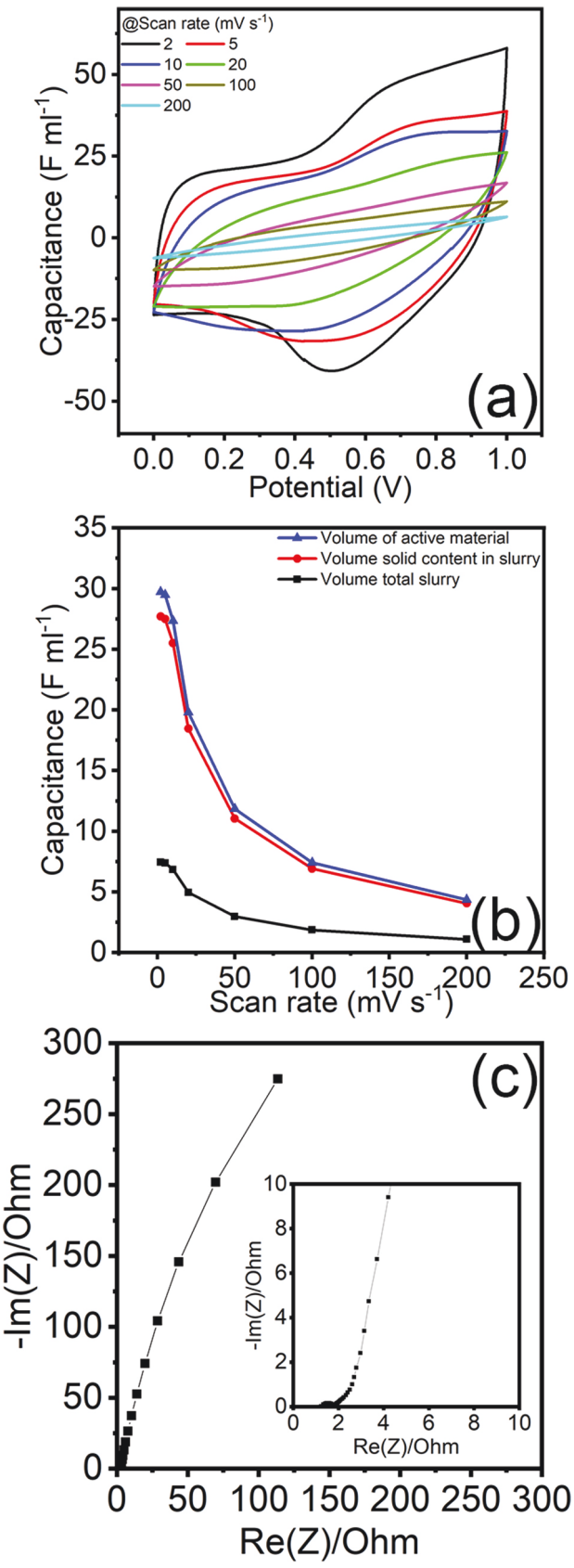

Fig. 7. CV of AC//MXene asymmetric flow capacitor with various scan rates (a); and variation of capacitance with scan rate for the asymmetric device (b); Nyquist plot from 1 MHz to 5 mHz for the AC//$Ti_3C_2T_x$ asymmetric device of 9.2:3.4 vol.% ($Ti_3C_2T_x$:CB at anode) & 35:0.8 vol.% (AC:CB at cathode) (c).

density despite its relatively small voltage window (0.4 V). On the other hand, the volumetric power density of the AC/$Ti_3C_2T_x$ asymmetric device is lower, however an improved energy density was achieved due to the voltage window (1 V).

Fig. 8(b) shows the gravimetric performance analysis for the same literature. As discussed earlier, due to the high density of multilayer $Ti_3C_2T_x$, the symmetric device exhibits poor gravimetric energy/power density performance. This is apparent in the asymmetric device assembly, which is comparable to previous literature due to the use of activated carbon as the cathode and low $Ti_3C_2T_x$ concentration in the device. The volumetric Ragone plot shows energy density values of 2.65 Wh l^{-1} (power density 47.32 W l^{-1}) for the symmetric device and 4.12 Wh l^{-1} (power density 31.73 W l^{-1}) for the asymmetric device. A gravimetric energy density of 6.47 Wh kg^{-1} (power density 49.77 W kg^{-1}) was achieved with the asymmetric device, which compares well to the previous work done in the field.

5. Conclusion

In this study, we have demonstrated the potential for $Ti_3C_2T_x$ to be used in suspension based electrochemical applications. $Ti_3C_2T_x$ was found to offer higher material packing in suspensions without compromising the flowability of the slurry, resulting in a better overall performance. Our findings show that the volumetric capacitance of $Ti_3C_2T_x$ in a symmetric configuration can reach 240 F ml^{-1}. However, the operating voltage window for the symmetric MXene devices was limited to 0.4 V, due to the poor electrochemical stability of MXenes at positive potentials. Despite a narrow potential window, the symmetric device still exhibited an energy density of 2.65 Wh l^{-1} (power density 47.82 W l^{-1}). To mitigate the narrow voltage window issue, an asymmetric device assembly consisting of $Ti_3C_2T_x$ as the negative and activated carbon as the positive electrode was also investigated. Despite using less $Ti_3C_2T_x$ to equilibrate the electrical conductivity of the asymmetric electrodes, it was shown that a volumetric energy density of 4.12 Wh l^{-1} (power density of 31.73 W l^{-1}) could be achieved, as the potential window could be expanded to 1 V.

This first attempt to use MXene in a suspension electrode capacitor suggests that $Ti_3C_2T_x$ holds great promise for use in flowable energy storage systems. Considering the limited voltage stability of $Ti_3C_2T_x$ under positive (anodic) potentials, hybrid/asymmetric devices offer a wider operating voltage and are a viable option. However, the capacitive performance in the asymmetric configuration also depends on the choice of the slurry material in the positive electrode. Hence, future work should focus on the development of suitable slurry materials with good rheological performance for positive electrodeto match the high charge storage capability of $Ti_3C_2T_x$. One possibility may be use of MXene systems that can work in positive potential window in a couple with $Ti_3C_2T_x$.

CRediT authorship contribution statement

Pushpendra Singh: Conception and design of study, Acquisition of data, Formal analysis, Drafting the manuscript, Approval of the version of the manuscript to be published. **Bilen Akuzum:** Conception and design of study, Acquisition of data, Formal analysis, Drafting the manuscript, Approval of the version of the manuscript to be published. **Christopher E. Shuck:** Acquisition of data, Formal analysis, Drafting the manuscript, Approval of the version of the manuscript to be published. **Kaushik Pal:** Conception and design of study, Formal analysis, Drafting the manuscript, Approval of the version of the manuscript to be published. **Yury Gogotsi:** Conception and design of study, Formal analysis, Drafting the manuscript, Approval of the version of the manuscript to be published. **E. Caglan Kumbur:** Conception and design of study, Formal analysis, Drafting the manuscript, Approval of the version of the manuscript to be published.

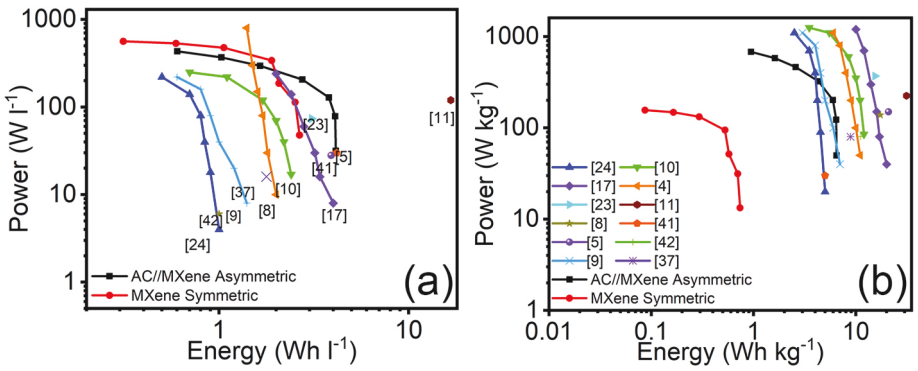

Fig. 8. Comparative Ragone plots for volumetric energy and power density variation with scan rates (a); gravimetric energy and power density variation with scan rates (b).

Declaration of competing interest

The authors declare that they have no known competing financial interests or personal relationships that could have appeared to influence the work reported in this paper.

Acknowledgments

The authors would like to thank the University Grant Commission (UGC) India and Fulbright-Nehru Doctoral research program funded by United States India Education Foundation -USIEF (Grant #2332/DR/2018–2019) for providing financial support. The authors also would like to acknowledge the support of the US National Science Foundation (Grant #2034108). Lastly, the authors would like to thank Mr. Ali Vala Mizrak, Dr. Lutfi Agartan, Dr. Narendra Kurra and Dr. Milan Jana for their valuable discussions and support.

Appendix A. Supplementary data

Supplementary data to this article can be found online at https://doi.org/10.1016/j.jpowsour.2021.230187.

References

[1] V. Presser, C.R. Dennison, J. Campos, K.W. Knehr, E.C. Kumbur, Y. Gogotsi, The electrochemical flow capacitor: a new concept for rapid energy storage and recovery, Adv. Energy Mater. (2012), https://doi.org/10.1002/aenm.201100768.
[2] M. Duduta, B. Ho, V.C. Wood, P. Limthongkul, V.E. Brunini, W.C. Carter, Y. M. Chiang, Semi-solid lithium rechargeable flow battery, Adv. Energy Mater. (2011), https://doi.org/10.1002/aenm.201100152.
[3] K.B. Hatzell, E. Iwama, A. Ferris, B. Daffos, K. Urita, T. Tzedakis, F. Chauvet, P. L. Taberna, Y. Gogotsi, P. Simon, Capacitive deionization concept based on suspension electrodes without ion exchange membranes, Electrochem. Commun. (2014), https://doi.org/10.1016/j.elecom.2014.03.003.
[4] K.B. Hatzell, L. Fan, M. Beidaghi, M. Boota, E. Pomerantseva, E.C. Kumbur, Y. Gogotsi, Composite manganese oxide percolating networks as a suspension electrode for an asymmetric flow capacitor, ACS Appl. Mater. Interfaces (2014), https://doi.org/10.1021/am501650q.
[5] C.R. Dennison, M. Beidaghi, K.B. Hatzell, J.W. Campos, Y. Gogotsi, E.C. Kumbur, Effects of flow cell design on charge percolation and storage in the carbon slurry electrodes of electrochemical flow capacitors, J. Power Sources (2014), https://doi.org/10.1016/j.jpowsour.2013.08.101.
[6] H. Chen, Y.C. Lu, A high-energy-density multiple redox semi-solid-liquid flow battery, Adv. Energy Mater (2016), https://doi.org/10.1002/aenm.201502183.
[7] E. Ventosa, D. Buchholz, S. Klink, C. Flox, L.G. Chagas, C. Vaalma, W. Schuhmann, S. Passerini, J.R. Morante, Non-aqueous semi-solid flow battery based on Na-ion chemistry. P2-type Na(x)Ni(0.22)Co(0.11)Mn(0.66)O(2)-NaTi2(PO4)3, Chem. Commun. (Camb) (2015), https://doi.org/10.1039/c4cc09597a.
[8] C. Zhang, K.B. Hatzell, M. Boota, B. Dyatkin, M. Beidaghi, D. Long, W. Qiao, E. C. Kumbur, Y. Gogotsi, Highly porous carbon spheres for electrochemical capacitors and capacitive flowable suspension electrodes, Carbon N. Y. (2014), https://doi.org/10.1016/j.carbon.2014.05.017.
[9] M. Boota, K.B. Hatzell, M. Alhabeb, E.C. Kumbur, Y. Gogotsi, Graphene-containing flowable electrodes for capacitive energy storage, Carbon N. Y. (2015), https://doi.org/10.1016/j.carbon.2015.04.020.
[10] M. Boota, K.B. Hatzell, E.C. Kumbur, Y. Gogotsi, Towards high-energy-density pseudocapacitive flowable electrodes by the incorporation of hydroquinone, ChemSusChem (2015), https://doi.org/10.1002/cssc.201402985.
[11] K.B. Hatzell, M. Beidaghi, J.W. Campos, C.R. Dennison, E.C. Kumbur, Y. Gogotsi, A high performance pseudocapacitive suspension electrode for the electrochemical flow capacitor, Electrochim. Acta (2013), https://doi.org/10.1016/j.electacta.2013.08.095.
[12] Z. Yang, J. Zhang, M.C.W. Kintner-Meyer, X. Lu, D. Choi, J.P. Lemmon, J. Liu, Electrochemical energy storage for green grid, Chem. Rev. (2011), https://doi.org/10.1021/cr100290v.
[13] B. Dunn, H. Kamath, J.-M. Tarascon, Electrical energy storage for the grid: a battery of choices, Science (2011), https://doi.org/10.1126/science.1212741.
[14] B. Akuzum, P. Singh, D.A. Eichfeld, L. Agartan, S. Uzun, Y. Gogotsi, E.C. Kumbur, Percolation characteristics of conductive additives for capacitive flowable (semi-solid) electrodes, ACS Appl. Mater. Interfaces (2020), https://doi.org/10.1021/acsami.9b19739.
[15] K.B. Hatzell, M. Boota, Y. Gogotsi, Materials for suspension (semi-solid) electrodes for energy and water technologies, Chem. Soc. Rev. (2015), https://doi.org/10.1039/c5cs00279f.
[16] J. Torop, F. Summer, V. Zadin, T. Koiranen, A. Jänes, E. Lust, A. Aabloo, Low concentrated carbonaceous suspensions assisted with carboxymethyl cellulose as electrode for electrochemical flow capacitor, Eur. Phys. J. E. (2019), https://doi.org/10.1140/epje/i2019-11766-2.
[17] T. Tomai, H. Saito, I. Honma, High-energy-density electrochemical flow capacitors containing quinone derivatives impregnated in nanoporous carbon beads, J. Mater. Chem. A (2017), https://doi.org/10.1039/C6TA08733G.
[18] M. Sarno, E. Ponticorvo, D. Scarpa, Ru and Os based new electrode for electrochemical flow supercapacitors, Chem. Eng. J. (2018), https://doi.org/10.1016/j.cej.2018.09.211.
[19] D.P. Dubal, D. Rueda-Garcia, C. Marchante, R. Benages, P. Gomez-Romero, Hybrid graphene-polyoxometalates nanofluids as liquid electrodes for dual energy storage in novel flow cells, Chem. Rec. (2018), https://doi.org/10.1002/tcr.201700116.
[20] W. Liu, N. Liu, Y. Shi, Y. Chen, C. Yang, J. Tao, S. Wang, Y. Wang, J. Su, L. Li, Y. Gao, A wire-shaped flexible asymmetric supercapacitor based on carbon fiber coated with a metal oxide and a polymer, J. Mater. Chem. A (2015), https://doi.org/10.1039/c5ta01105a.
[21] K. Aruchamy, R. Nagaraj, H.M. Manohara, M.R. Nidhi, D. Mondal, D. Ghosh, S. K. Nataraj, One-step green route synthesis of spinel $ZnMn_2O_4$ nanoparticles decorated on MWCNTs as a novel electrode material for supercapacitor, Mater. Sci. Eng. B Solid-State Mater. Adv. Technol. (2020), https://doi.org/10.1016/j.mseb.2019.114481.
[22] H. Shi, Activated carbons and double layer capacitance, Electrochim. Acta (1996), https://doi.org/10.1016/0013-4686(95)00416-5.
[23] J.W. Campos, M. Beidaghi, K.B. Hatzell, C.R. Dennison, B. Musci, V. Presser, E. C. Kumbur, Y. Gogotsi, Investigation of carbon materials for use as a flowable electrode in electrochemical flow capacitors, Electrochim. Acta 98 (2013) 123–130, https://doi.org/10.1016/j.electacta.2013.03.037.
[24] M. Boota, K.B. Hatzell, M. Beidaghi, C.R. Dennison, E.C. Kumbur, Y. Gogotsi, Activated carbon spheres as a flowable electrode in electrochemical flow capacitors, J. Electrochem. Soc. 161 (2014) A1078–A1083, https://doi.org/10.1149/2.072406jes.
[25] K.B. Hatzell, M.C. Hatzell, K.M. Cook, M. Boota, G.M. Housel, A. McBride, E. C. Kumbur, Y. Gogotsi, Effect of oxidation of carbon material on suspension electrodes for flow electrode capacitive deionization, Environ. Sci. Technol. (2015), https://doi.org/10.1021/es5055989.
[26] J. Lee, D. Weingarth, I. Grobelsek, V. Presser, Use of surfactants for continuous operation of aqueous electrochemical flow capacitors, Energy Technol. (2016), https://doi.org/10.1002/ente.201500243.
[27] J. Zhang, N. Kong, S. Uzun, A. Levitt, S. Seyedin, P.A. Lynch, S. Qin, M. Han, W. Yang, J. Liu, X. Wang, Y. Gogotsi, J.M. Razal, Scalable manufacturing of free-standing, strong $Ti_3C_2T_x$ MXene films with outstanding conductivity, Adv. Mater. (2020), https://doi.org/10.1002/adma.202001093.

[28] B. Anasori, M.R. Lukatskaya, Y. Gogotsi, 2D metal carbides and nitrides (MXenes) for energy storage, Nat. Rev. Mater. (2017), https://doi.org/10.1038/natrevmats.2016.98.
[29] M. Naguib, M. Kurtoglu, V. Presser, J. Lu, J. Niu, M. Heon, L. Hultman, Y. Gogotsi, M.W. Barsoum, Two-dimensional nanocrystals produced by exfoliation of Ti_3AlC_2, Adv. Mater. (2011), https://doi.org/10.1002/adma.201102306.
[30] G. Deysher, C.E. Shuck, K. Hantanasirisakul, N.C. Frey, A.C. Foucher, K. Maleski, A. Sarycheva, V.B. Shenoy, E.A. Stach, B. Anasori, Y. Gogotsi, Synthesis of Mo_4VAlC_4 MAX phase and two-dimensional Mo_4VC_4 MXene with five atomic layers of transition metals, ACS Nano (2020), https://doi.org/10.1021/acsnano.9b07708.
[31] N.K. Chaudhari, H. Jin, B. Kim, D. San Baek, S.H. Joo, K. Lee, MXene: an emerging two-dimensional material for future energy conversion and storage applications, J. Mater. Chem. A (2017), https://doi.org/10.1039/c7ta09094c.
[32] M. Ghidiu, M.R. Lukatskaya, M.Q. Zhao, Y. Gogotsi, M.W. Barsoum, Conductive two-dimensional titanium carbide "clay" with high volumetric capacitance, Nature (2015), https://doi.org/10.1038/nature13970.
[33] M.R. Lukatskaya, O. Mashtalir, C.E. Ren, Y. Dall'Agnese, P. Rozier, P.L. Taberna, M. Naguib, P. Simon, M.W. Barsoum, Y. Gogotsi, Cation intercalation and high volumetric capacitance of two-dimensional titanium carbide, Science 80 (2013), https://doi.org/10.1126/science.1241488.
[34] B. Akuzum, K. Maleski, B. Anasori, P. Lelyukh, N.J. Alvarez, E.C. Kumbur, Y. Gogotsi, Rheological characteristics of 2D titanium carbide (MXene) dispersions: a guide for processing MXenes, ACS Nano (2018), https://doi.org/10.1021/acsnano.7b08889.
[35] C.E. Shuck, A. Sarycheva, M. Anayee, A. Levitt, Y. Zhu, S. Uzun, V. Balitskiy, V. Zahorodna, O. Gogotsi, Y. Gogotsi, Scalable synthesis of $Ti_3C_2T_x$ MXene, Adv. Eng. Mater. (2020), https://doi.org/10.1002/adem.201901241.
[36] M. Alhabeb, K. Maleski, B. Anasori, P. Lelyukh, L. Clark, S. Sin, Y. Gogotsi, Guidelines for synthesis and processing of two-dimensional titanium carbide ($Ti_3C_2T_x$ MXene), Chem. Mater. (2017), https://doi.org/10.1021/acs.chemmater.7b02847.
[37] M. Tian, Y. Sun, C.(John, Zhang, J. Wang, W. Qiao, L. Ling, D. Long, Enabling high-rate electrochemical flow capacitors based on mesoporous carbon microspheres suspension electrodes, J. Power Sources (2017), https://doi.org/10.1016/j.jpowsour.2017.08.001.
[38] B. Akuzum, D.D. Hudson, D.A. Eichfeld, C.R. Dennison, L. Agartan, Y. Gogotsi, E. C. Kumbur, Reticulated carbon electrodes for improved charge transport in electrochemical flow capacitors, J. Electrochem. Soc. (2018), https://doi.org/10.1149/2.0361811jes.
[39] D. Pinto, B. Anasori, H. Avireddy, C.E. Shuck, K. Hantanasirisakul, G. Deysher, J. R. Morante, W. Porzio, H.N. Alshareef, Y. Gogotsi, Synthesis and electrochemical properties of 2D molybdenum vanadium carbides-solid solution MXenes, J. Mater. Chem. A (2020), https://doi.org/10.1039/d0ta01798a.
[40] A. Rommerskirchen, A. Kalde, C.J. Linnartz, L. Bongers, G. Linz, M. Wessling, Unraveling charge transport in carbon flow-electrodes: performance prediction for desalination applications, Carbon N. Y. (2019), https://doi.org/10.1016/j.carbon.2019.01.053.
[41] S. Porada, J. Lee, D. Weingarth, V. Presser, Continuous operation of an electrochemical flow capacitor, Electrochem. Commun. (2014), https://doi.org/10.1016/j.elecom.2014.08.023.
[42] B. Akuzum, L. Agartan, J. Locco, E.C. Kumbur, Effects of particle dispersion and slurry preparation protocol on electrochemical performance of capacitive flowable electrodes, J. Appl. Electrochem. (2017), https://doi.org/10.1007/s10800-017-1046-5.